

# Probing multiferroicity and spin-spin interactions via dielectric measurements on Y-doped $\text{HoMnO}_3$ in high magnetic fields

R. Vasic, H. D. Zhou, E. Jobiliong, C. R. Wiebe, and J. S. Brooks

*Department of Physics and National High Magnetic Field Laboratory, Florida State University, Tallahassee, Florida 32310, USA*

(Received 28 July 2006; revised manuscript received 22 November 2006; published 26 January 2007)

The magnetic field dependent phase diagrams of the ferrielectric material  $\text{Ho}_{1-x}\text{Y}_x\text{MnO}_3$  have been investigated for  $x=0, 0.6,$  and  $0.8$  for fields directed along both the  $ab$  in-plane and the  $c$ -axis directions. Dielectric measurements are used to map out the reentrant temperature-magnetic field phase transitions which involve in-plane Mn spin rotations in the antiferromagnetic state below the Néel temperature. We describe this behavior in terms of the interaction of the Ho sublattice spin system with the underlying, robust  $\text{YMnO}_3$  antiferromagnetic triangular lattice, where the Ho-Y spin interactions are highly sensitive to concentration and field direction.

DOI: [10.1103/PhysRevB.75.014436](https://doi.org/10.1103/PhysRevB.75.014436)

PACS number(s): 75.47.Lx, 77.80.-e

## I. INTRODUCTION

The rare-earth hexagonal materials  $\text{RMnO}_3$  ( $R$  represents from Ho to Lu and Y)<sup>1</sup> have attracted considerable recent attention due to the uncommon coexistence of coupled ferrielectric and antiferromagnetic ordering.<sup>2</sup> Exemplary in the understanding of this family of compounds is  $\text{YMnO}_3$ , which has a ferrielectric transition at  $T_C=900$  K.<sup>3-5</sup> This gives rise to a small distortion of the two-dimensional networks of triangular  $\text{Mn}^{3+}$  ( $S=2$ ) ions out of the basal plane. In principle, the Mn-Mn spin interactions are highly frustrated, but this lattice distortion relieves some of the frustration, and results in an antiferromagnetic ordering at 70 K with a 120 degree spin structure.<sup>6</sup> Hence, the ferrielectric and magnetic order can coexist with a strong coupling between the two disparate phenomena.<sup>7</sup>

The compound  $\text{HoMnO}_3$ , where the nonmagnetic  $\text{Y}^{3+}$  ions have been replaced with  $\text{Ho}^{3+}$ , is a more complex system due to the additional interaction of  $\text{Ho}^{3+}$  spins.<sup>2</sup> Although the ferrielectric temperature ( $T_C=875$  K) does not change significantly from  $\text{YMnO}_3$ , there is a series of lower temperature magnetic transitions.<sup>8</sup> The  $\text{Mn}^{3+}$  spins order antiferromagnetically<sup>1</sup> at  $T_N=76$  K. There is a subsequent spin reorientation transition between 40 K and 33 K ( $T_{SR}$ ), which is accompanied by a small moment forming on the Ho site.<sup>10-14</sup> The Ho spins themselves order completely at  $T_{Ho}=5$  K, where a second Mn spin reorientation occurs.<sup>9</sup> The complete magnetic structure is still a matter of debate, but recent measurements have shown that (1) at  $T_N$ , the Mn spins are in a 120 degree antiferromagnetic structure; (2) at  $T_{SR}$  there is a 90 degree rotation of these spins accompanied by a partial ordering of the Ho spins along the  $c$  direction; (3) at  $T_{Ho}$ , there is a final reorientation of the Mn spins in the basal plane, with a complete AF ordering of the Ho spins.<sup>2,10</sup> At temperatures at and below  $T_{Ho}$ , recent measurements on flux grown single crystals have shown that additional phases appear as a function of magnetic field.<sup>15-17</sup>

Recent work on these  $\text{RMnO}_3$  compounds has been focused on the magnetic phases at low temperatures and the coupling between the ferrielectric and magnetic ordering of  $\text{Mn}^{3+}$  ions.<sup>7,16,18-22</sup> Due to the coupling of the ferrielectric and magnetic order parameters to the lattice, the dielectric

effect is a useful probe to map the magnetic phase. Most of the recently reported dielectric measurements have been performed on  $\text{HoMnO}_3$  and  $\text{YMnO}_3$  with low applied magnetic fields along the  $c$  axis. In the present work, we focus on dielectric measurements on single crystals of  $\text{Ho}_{1-x}\text{Y}_x\text{MnO}_3$  and  $\text{HoMn}_{1-y}\text{Ga}_y\text{O}_3$  with applied magnetic field (up to 13 T) along both the  $ab$  in-plane and the  $c$ -axis directions. The emphasis is (i) to see how the magnetic phases vary with Y and Ga doping; (ii) to explore the anisotropic high magnetic field properties of multiferroicity in  $\text{RMnO}_3$ .

## II. EXPERIMENT

Single crystals of  $\text{HoMnO}_3$ ,  $\text{Ho}_{1-x}\text{Y}_x\text{MnO}_3$  ( $x=0, 0.6, 0.8$ ) and  $\text{HoMn}_{1-y}\text{Ga}_y\text{O}_3$  ( $y=0.1$ ) were grown by a traveling-solvent-floating zone (TSFZ) technique.<sup>23</sup> Samples with typical dimensions  $0.5 \times 0.5 \times 5.0$  mm<sup>3</sup> were oriented, cut and polished for dielectric measurements with parallel plate silver electrodes normal to the  $c$  direction. A standard  $ac$  capacitance bridge method was employed where the rms electric field amplitude applied between the plates in the  $c$  direction was 50 V/cm, substantially less than the  $10^5$  V/cm field used to stabilize the polarized Ho state.<sup>14</sup> The real (capacitive,  $C$ ) and loss (dissipative,  $D$ ) signals were measured at 100 kHz vs temperature in both low field superconducting and high field resistive magnets at the National High Magnetic Field Laboratory. In all cases presented here the  $ac$  electrical field was parallel to the  $c$  axis. The magnetic field anisotropy was measured simultaneously for two samples of each Y concentration, cut from the same crystal to compare directly anisotropic effects of the magnetic field in  $ab$  plane and  $c$  direction. To avoid strong torque effects, care was taken to affix the samples to avoid movement in high magnetic fields.

## III. RESULTS

The transitions where Mn spin rotations occur can be observed by a number of different methods, including magnetization,  $ac$  magnetic susceptibility,<sup>24</sup> specific heat,<sup>11</sup> neutron scattering,<sup>10,13</sup> optical second harmonic generation,<sup>2,9,14,15,25</sup> lattice distortions,<sup>16</sup> thermal conductivity,<sup>26</sup> and due to the

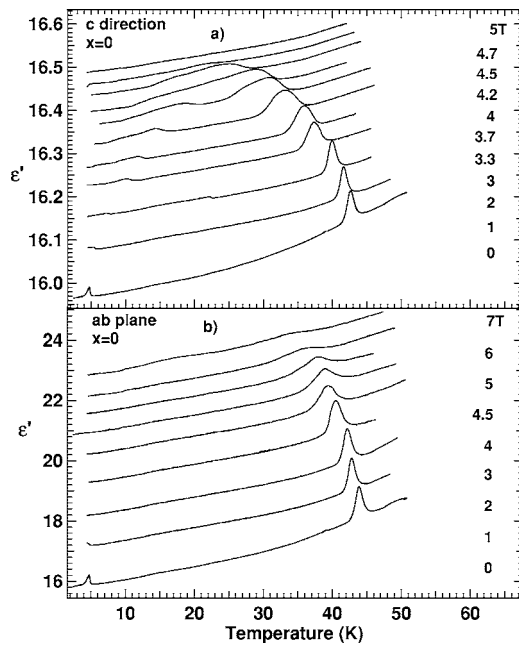


FIG. 1. Temperature dependence of real part of dielectric constant for  $\text{Ho}_{1-x}\text{Y}_x\text{MnO}_3$  ( $x=0$ ) for different magnetic fields. For  $B > 0$ , the curves are shifted upwards by arbitrary amounts. (a)  $B \parallel c$ . (b)  $B \parallel ab$ .

ferrielectric and magnetic coupling, dielectric measurements.<sup>16,19</sup> Our results for the two field orientations,  $B \parallel c$  and  $B \parallel ab$  are shown in Figs. 1–3 for  $\text{Ho}_{1-x}\text{Y}_x\text{MnO}_3$  and in Fig. 4 for  $\text{HoMn}_{0.9}\text{Ga}_{0.1}\text{O}_3$ . All data show the signature (peak in the dielectric constant) and field dependence of the higher temperature  $T_{\text{SR}}$  transition, and the lower temperature

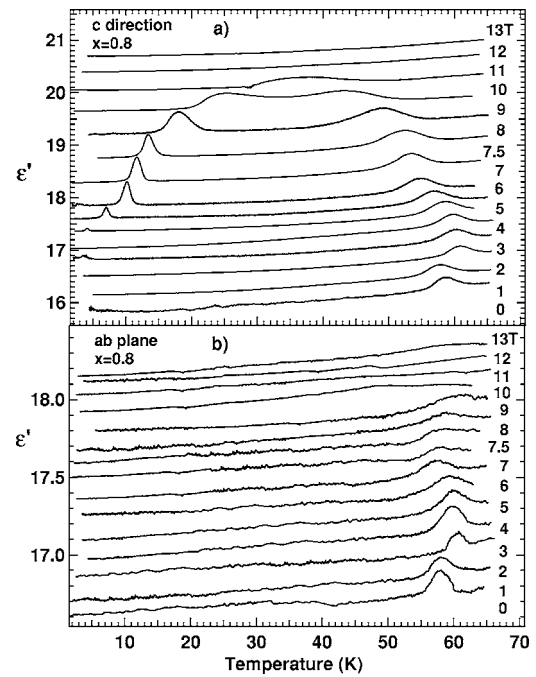


FIG. 3. Temperature dependence of real part of dielectric constant for  $\text{Ho}_{1-x}\text{Y}_x\text{MnO}_3$  ( $x=0.8$ ) for different magnetic fields. For  $B > 0$ , the curves are shifted upwards by arbitrary amounts. (a)  $B \parallel c$ . (b)  $B \parallel ab$ .

$T_{\text{Ho}}$  transition is also evident in some cases. (Our data do not extend to lower temperatures where additional phases<sup>15,16</sup> are observed.) The measured value of the dielectric constant for all samples was approximately 16, in agreement with other studies.<sup>16,19,22</sup>

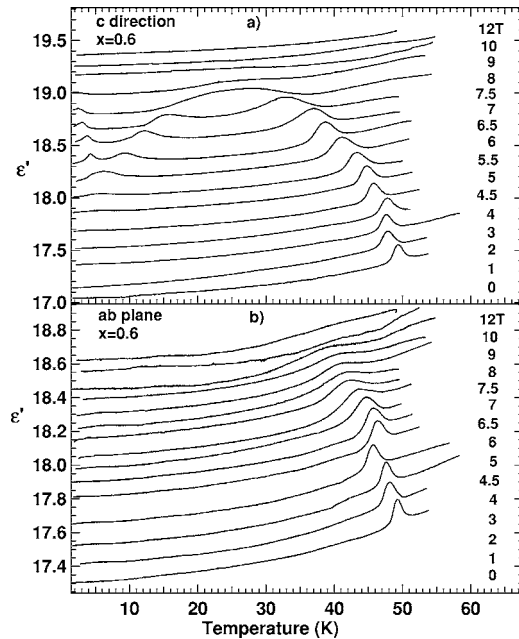


FIG. 2. Temperature dependence of real part of dielectric constant for  $\text{Ho}_{1-x}\text{Y}_x\text{MnO}_3$  ( $x=0.6$ ) for different magnetic fields. For  $B > 0$ , the curves are shifted upwards by arbitrary amounts. (a)  $B \parallel c$ . (b)  $B \parallel ab$ .

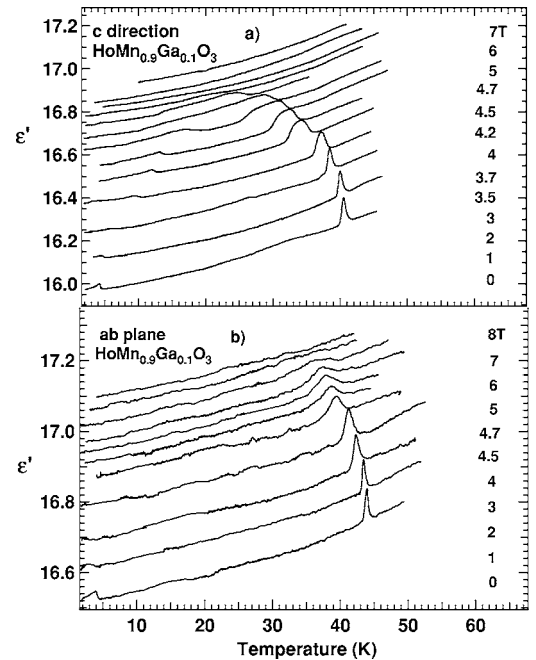


FIG. 4. Temperature dependence of real part of dielectric constant for  $\text{HoMn}_{0.9}\text{Ga}_{0.1}\text{O}_3$  ( $y=0.1$ ) for different magnetic fields. For  $B > 0$ , the curves are shifted upwards by arbitrary amounts. (a)  $B \parallel c$ . (b)  $B \parallel ab$ .

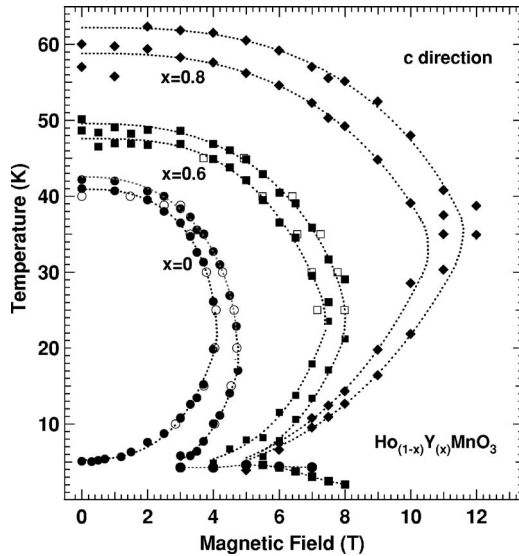


FIG. 5. Magnetic field-temperature phase diagrams for  $\text{Ho}_{1-x}\text{Y}_x\text{MnO}_3$  ( $x=0;0.6;0.8$ ) for magnetic field applied in the  $c$  direction. Solid and open symbols represent temperature and field sweeps, respectively. (Dashed lines are guides to the eye.) Circles,  $x=0$ ; squares,  $x=0.6$ ; diamonds,  $x=0.8$ . The intermediate phase boundary widths correspond to the dielectric constant peak half-widths. The phase diagram for  $\text{HoMn}_{0.9}\text{Ga}_{0.1}\text{O}_3$  for  $B\parallel c$  (not shown) is indiscernible from that for pure  $\text{HoMnO}_3$ .

In Fig. 5 (for  $B\parallel c$ ) and Fig. 6 (for  $B\parallel ab$ ) we summarize the field and temperature dependent dielectric peak signatures observed for all samples and field directions. The most prominent features are the  $T_{\text{SR}}$  and  $T_{\text{Ho}}$  phase boundaries. We focus first on the  $\text{HoMnO}_3$  (i.e.,  $x=0$ ) phase diagram in Fig. 5, where the full-width at half-maxima of the dielectric peaks have been used to determine the widths of the transitions. The data show overall agreement with previous determina-

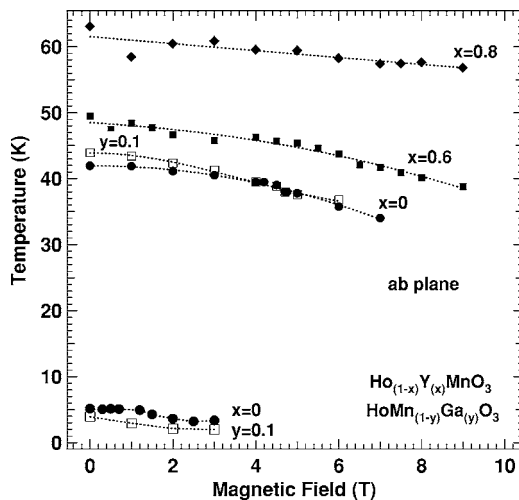


FIG. 6. Magnetic field-temperature phase diagrams for  $\text{Ho}_{1-x}\text{Y}_x\text{MnO}_3$  ( $x=0;0.6;0.8$ ) and  $\text{HoMn}_{1-y}\text{Ga}_y\text{O}_3$  ( $y=0.1$ ) for magnetic field applied in the  $ab$  plane direction. All data are from temperature sweeps, and only the dielectric peak locations are indicated. (Dashed lines are guides to the eye.) Circles,  $x=0$ ; squares,  $x=0.6$ ; diamonds,  $x=0.8$ ; open squares,  $y=0.1$ .

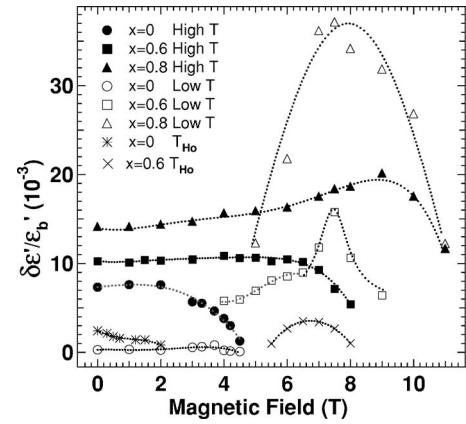


FIG. 7. Field dependence of the relative change of the dielectric peak heights  $\delta\epsilon'/\epsilon'_b$  at the  $T_{\text{SR}}$  and  $T_{\text{Ho}}$  transitions for the  $\text{Ho}_{1-x}\text{Y}_x\text{MnO}_3$  compounds for  $B\parallel c$ . (Here  $\epsilon'_b$  is the extrapolated background at the peak position.) Note that the peak locations also vary with temperature, as indicated in the legend as “high” and “low” for the upper and lower temperature branches of the  $T_{\text{SR}}$  phase boundaries, respectively (similarly for  $T_{\text{Ho}}$ ).

tions of the  $B\parallel c$  “reentrant” phase diagram.<sup>19</sup> In Fig. 6, referring first to the  $x=0$  data phase diagram for the  $B\parallel ab$ -plane data, we find that the slope  $dT_{\text{SR}}/d(B\parallel ab)$  is significantly less, that  $T_{\text{SR}}$  persists to significantly higher fields, and that the reentrant character of the phase diagram is nearly gone. (In Fig. 6 only the peak values for  $T_{\text{SR}}$  and  $T_{\text{Ho}}$  are plotted.)

Turning next to the doping study, we find that for  $B\parallel c$  (Fig. 5)  $T_{\text{SR}}$  increases with increasing Y concentration, and that in general the reentrant phase boundaries expand in both their range of temperature and field. For  $B\parallel ab$ ,  $dT_{\text{SR}}/d(B\parallel ab)$  decreases with increasing Y concentration, and for  $x=0.6$  and  $0.8$ , the lower transition normally attributed to  $T_{\text{Ho}}$  vanishes, and the reentrant phase boundary is gone. For  $\text{HoMn}_{0.9}\text{Ga}_{0.1}\text{O}_3$  which represents a small non-magnetic substitution of Ga on the Mn site, we found that Ga ( $y=0.1$ ) increases  $T_{\text{SR}}$  and decreases  $T_{\text{Ho}}$  (Fig. 6) expanding the  $P6_3cm$  phase region. With the Ga alloy it helps to show the magnetic properties and alloy properties of  $\text{RMnO}_3$ . The Ga alloy data also emphasize the role of Mn-Mn in-plane interactions (Fig. 6).

There are some other aspects of the data that are noteworthy. The widths of the peaks in the phase diagram (Fig. 5) have been interpreted as representing an intermediate “INT” phase by Lorenz *et al.*<sup>11</sup> Not only the widths, but the amplitudes of the peaks in the dielectric response at the transitions exhibit a significant dependence on temperature, field, and Y concentration. In Fig. 7 we summarize the behavior of the relative change of the dielectric peak heights vs their loci in magnetic field and temperature for the different alloy samples. Most notably, the peak heights are generally non-monotonic with field and temperature, and show pronounced maxima for the more concentrated Y samples. For  $x=0$  the dielectric constant peak monotonically decreases with magnetic field. Systems with  $x=0.6$ , and  $x=0.8$  at lower  $T_{\text{SR}}$  show a high relative change of the dielectric constant at around 8 T. In addition, the half-width of this function

changes with doping (4 T for  $x=0.8$ , and 1 T for  $x=0.6$ , respectively). Similarly, the holmium ordering  $T_{\text{Ho}}$  for more Y diluted system shows nonmonotonic field dependence in contrast to the pure system (Fig. 7). For  $x=0.6$  the increase of the size of the peak is correlated to the decrease in the slope of the phase diagram  $dT_{\text{SR}}/d(B\parallel ab)$  (Fig. 5). Finally, for  $x=0.8$  the signature of holmium ordering is absent, but the peak in relative change of dielectric constant at high  $T_{\text{SR}}$  emerges at around 9 T. The field and/or temperature dependence of the  $T_{\text{SR}}$  transition widths (not plotted, but evident by examination of the  $T$ - $B$  widths of the reentrant phase boundaries in Fig. 5), also show a dependence on Y concentration, temperature, and magnetic field.

#### IV. DISCUSSION

The main results of the present work are that (1) the in-plane magnetic field greatly affects the influence of holmium on the spin-rotation transitions; and (2) for increasing Y concentration ( $x \rightarrow 1$ ) in  $\text{Ho}_{1-x}\text{Y}_x\text{MnO}_3$ , the  $T_{\text{SR}}$  transition approaches  $T_{\text{N}}$  and the  $P\bar{6}_3cm$  phase region expands, which is the same  $P\bar{6}_3cm$  symmetry that is observed in pure  $\text{YMnO}_3$  below  $T_{\text{N}}$ .<sup>14</sup> Our results, as represented in Figs. 5 and 6, show that for either/or in-plane magnetic field and reduced Ho concentration, the lower temperature reentrant phase boundary is removed. Only in the case for  $x=0$  is  $T_{\text{Ho}}$  evident for  $B\parallel ab$ . Below we discuss the behavior of the dielectric constant at  $T_{\text{SR}}$ , and the significance of the alloy and field direction studies in turn.

##### A. Dielectric response at $T_{\text{SR}}$

The origin of the spin rotation is due to the presence of the Ho spin sublattice, where the tendency of the Ho to form an ordered state is accompanied by in-plane adjustments of the original native  $P\bar{6}_3cm$  symmetry of the pure  $\text{YMnO}_3$  triangular lattice AFM order below  $T_{\text{N}}$ . The dielectric measurements show an increase in dielectric constant as the reentrant phase boundaries are crossed between the  $P\bar{6}_3cm$  and  $P\bar{6}_3c\bar{m}$  symmetries. Following the arguments of Lorenz *et al.*<sup>11</sup> it is expected that a lower symmetry  $P\bar{6}_3$  Mn spin configuration is present as the spins rotate from one configuration to the other. This intermediate state causes the dielectric constant to increase; indicating additional spin-lattice strain effects are present during the transition.<sup>27</sup> However, the dielectric constant is nearly the same in either of the adjacent  $P\bar{6}_3c\bar{m}$  and  $P\bar{6}_3cm$  phases. Theoretical progress has been made in describing the electric polarization susceptibility change at  $T_{\text{N}}$  due to coupling between AFM and ferroelectric ordering.<sup>21</sup> A similar description for the  $T_{\text{SR}}$  transition has been treated.<sup>22,25</sup> It is reasonable to expect that the change in the dielectric constant is mainly coupled to the  $S_i S_j$  term in the magneto-electric coupling Hamiltonian.<sup>20</sup> Here  $S_i$  and  $S_j$  are the Mn spins on nearest-neighbor sites, and hence for any rotation away from either of the two ground state spin orientations, the free energy will increase. The transition across the  $T_{\text{SR}}$  boundary therefore is similar to a two level system with an energy barrier associated with the intermediate state. The field and temperature dependence of the peaks in the dielec-

tric constant shown in Fig. 7 should provide guidance for future theoretical work to describe the behavior of the dielectric signal as the  $T_{\text{SR}}$  boundaries are crossed.

##### B. Significance of the doping studies

As discussed above, the increase in Y (decrease in Ho) concentration increases the region of the  $P\bar{6}_3cm$  phase which is also the symmetry of pure  $\text{YMnO}_3$  below  $T_{\text{N}}$ . By reducing the Ho concentration, it also takes larger  $B\parallel c$  magnetic fields to induce the  $P\bar{6}_3c\bar{m}$  phase. Given the nature of the sublattice spin structure, it is not clear how reducing the Ho concentration increases the magnetic field at which the  $P\bar{6}_3c\bar{m}$  sublattice magnetic order returns the  $P\bar{6}_3cm$  configuration. At  $x=0.8$ , the maximum field required to suppress ordering is approximately 10 T, compared to the  $x=0$  case where the maximum field is about 4 T. This may be understood with the observation that it is the Ho moments, partially oriented along the  $c$  direction, which cause the spin reorientation transition. Reducing the density of the Ho spins through Y substitution would result in a higher field for the Mn spin reorientation transition since the two sublattices are coupled together (through the introduction of spin-flip transitions out of the basal plane).

Recent neutron scattering results have shown that the anisotropy of the spin wave spectrum at low temperatures increases greatly due to the presence of ordered holmium, and drives the spin reorientation transition.<sup>10</sup> Ga ( $y=0.1$ ) doping reduces the antiferromagnetic ordering of Mn sublattice, resulting in the increase of  $T_{\text{SR}}$  and the decrease of  $T_{\text{Ho}}$ .<sup>23</sup> The slight decrease in Ho ordering temperature is one more indication of mutual Ho-Mn interactions that drive the spin reorientation and the rare-earth ordering. The rare-earth ordering (i.e.,  $T_{\text{Ho}}$ ) is also suppressed with decreasing Ho concentration, and this seems natural since the rare-earth nearest-neighbor interactions will be reduced. Due to the  $\sim 4$  K limit of our investigation, we did not explore the complicated low- $T$  phase diagram for  $\text{HoMnO}_3$  reported by other research groups.<sup>11,15</sup> We note that our spin reorientation temperature for  $\text{HoMnO}_3$  is higher than those reported in these previous studies ( $T_{\text{SR}}=42$  K vs 33 K), where crystals were flux grown. In the present case we used single crystals, grown by the floating zone method, and this may account for the higher  $T_{\text{SR}}$  values. We do however confirm the phase line near 5 K due to the rare-earth Ho ordering, and also the apparent widening of the ‘‘INT’’ region for  $x=0$  at low temperatures. This is within a region of phase space where neutron experiments see a continuous change in magnetic Bragg peak intensity (i.e., as the spins change orientation from one orientation to the next).<sup>2,10</sup>

##### C. Significance of the magnetic field direction

The Mn spins within the  $ab$  plane are severely frustrated, and large fields are needed to decouple them. Hence it is unlikely that in the range of magnetic field studied here the Mn spins were realigned solely due to the external field. Rather, it is most likely the magnetic field interaction with the Ho spin system, which is further coupled to the Mn spins, which drives the transitions. Since the Ho magnetic sublat-

tice spin orientations are along the  $c$  axis, a magnetic field applied in the  $ab$  plane will involve various types of antiferromagnetic polarization effects (spin-flop/spin-flip). Whereas for  $B\parallel c$  the reentrant phases are still present, it is evident from Fig. 6 that for  $B\parallel ab$ , the reentrance of the  $P\bar{6}_3cm$  phase at temperatures below the first  $T_{SR}$  transition is completely suppressed. Hence for  $B\parallel ab$ , the interaction of the magnetic field with the Ho system must be considerably stronger. In Fig. 6 the phase line for  $x=0$  near 5 K is  $T_{Ho}$ , which is suppressed for increasing field, and above 3 T, there is no discernable transition at  $T_{Ho}$ . This gives a rough estimate of the interactions between the Ho moments, which suggests an energy scale of about 1.8 meV (since the transition of  $T_{Ho}$  disappears around 3 T, we calculated the energy scale of the  $T_{Ho}$  interactions  $E=g_J\mu_B B$ , using  $J=8$ ). This is remarkably close to the first crystal field level of Ho as determined by neutron scattering [1.5(1) meV], providing a mechanism for inducing spin-flip transitions for the Ising-type Ho moments.<sup>10</sup>

## V. SUMMARY AND CONCLUSIONS

We have shown that by modifying the influence of the Ho sublattice by either nonmagnetic substitution for Ho, or with

in-plane magnetic fields, the mechanism that favors the  $P\bar{6}_3cm$  state is suppressed and the  $P\bar{6}_3cm$  characteristic of the pure  $YMnO_3$  system emerges. Maxima in peak height of the dielectric constant are correlated with the edges of the revised  $T_{SR}/B$  phase diagram. To fully understand these effects, a microscopic model is needed which includes a description of how the magnetic field (applied in different directions) affects the correlated Ho and Mn spin sublattices. Further experimental work to characterize the nature of the spin systems vs magnetic field direction and alloy control, particularly neutron scattering and second harmonic generation studies, would be very useful to better understand these complex interacting spin systems.

## ACKNOWLEDGMENTS

This research was sponsored by the National Nuclear Security Administration under the Stewardship Science Academic Alliances program through DOE Research Grant No. DE-FG03-03NA00066 (E.J.), NSF Grants Nos. DMR0203532 and DMR0602859 (J.S.B.), and the NHMFL is supported by contractual agreement between the National Science Foundation through NSF Grant No. DMR0449569 and the State of Florida.

- 
- <sup>1</sup>M. Fiebig, Th. Lottermoser, and R. V. Pisarev, *J. Appl. Phys.* **93**, 8194 (2003).
- <sup>2</sup>See, for example, M. Fiebig, Th. Lottermoser, D. Fröhlich, A. V. Goltsev, and R. V. Pisarev, *Nature (London)* **419**, 818 (2002).
- <sup>3</sup>F. Bertaut, P. Fang, and P. Forrat, *C. R. Hebd. Seances Acad. Sci.* **256**, 1958 (1963).
- <sup>4</sup>T. Lonkai, D. G. Tomuta, U. Amann, J. Ihringer, R. W. Hendriks, D. M. Tobbens, and J. A. Mydosh, *Phys. Rev. B* **69**, 134108 (2004).
- <sup>5</sup>B. B. Van Aken, T. T. M. Palstra, A. Filippetti, and N. A. Spaldin, *Nat. Mater.* **3**, 164 (2004).
- <sup>6</sup>Z. J. Huang, Y. Cao, Y. Y. Sun, Y. Y. Xue, and C. W. Chu, *Phys. Rev. B* **56**, 2623 (1997).
- <sup>7</sup>N. A. Hill, *J. Phys. Chem. B* **104**, 6694 (2000).
- <sup>8</sup>P. Coeuré, P. Guinet, J. C. Peuzin, G. Buisson, and E. F. Bertaut, in *Proceedings of the International Meeting on Ferroelectricity*, edited by V. Dvorák, A. Fousková, and P. Glogar (Institute of Physics of the Czechoslovak Academy of Science, Prague, 1966), Vol. 1, pp. 332–340.
- <sup>9</sup>Th. Lottermoser, Th. Lonkai, U. Amann, D. Hohlwein, J. Ihringer, and M. Fiebig, *Nature (London)* **430**, 541 (2004).
- <sup>10</sup>O. P. Vajk, M. Kenzelmann, J. W. Lynn, S. B. Kim, and S.-W. Cheong, *Phys. Rev. Lett.* **94**, 087601 (2005).
- <sup>11</sup>B. Lorenz, F. Yen, M. M. Gospodinov, and C. W. Chu, *Phys. Rev. B* **71**, 014438 (2005).
- <sup>12</sup>A. Muñoz, J. A. Alonso, M. J. Martínez-Lope, M. T. Casáis, J. L. Martínez, and M. T. Fernández-Díaz, *Chem. Mater.* **13**, 1497 (2001).
- <sup>13</sup>Th. Lonkai, D. Hohlwein, J. Ihringer, and W. Prandl, *Appl. Phys. A: Mater. Sci. Process.* **A74**, 843 (2002).
- <sup>14</sup>M. Fiebig, D. Fröhlich, K. Kohn, St. Leute, Th. Lottermoser, V. Pavlov, and R. V. Pisarev, *Phys. Rev. Lett.* **84**, 5620 (2000).
- <sup>15</sup>M. Fiebig, C. Degenhardt, and R. V. Pisarev, *J. Appl. Phys.* **91**, 8867 (2002).
- <sup>16</sup>F. Yen, C. R. de la Cruz, B. Lorenz, Y. Y. Sun, Y. Q. Wang, M. M. Gospodinov, and C. W. Chu, *Phys. Rev. B* **71**, 180407(R) (2005).
- <sup>17</sup>M. Fiebig, D. Fröhlich, Th. Lottermoser, and K. Kohn, *Appl. Phys. Lett.* **77**, 4401 (2000).
- <sup>18</sup>Seongsu Lee, A. Pirogov, Jung Hoon Han, J. -G. Park, A. Hoshikawa, and T. Kamiyama, *Phys. Rev. B* **71**, 180413(R) (2005).
- <sup>19</sup>B. Lorenz, A. P. Litvinchuk, M. M. Gospodinov, and C. W. Chu, *Phys. Rev. Lett.* **92**, 087204 (2004).
- <sup>20</sup>T. Katsufuji, S. Mori, M. Masaki, Y. Moritomo, N. Yamamoto, and H. Takagi, *Phys. Rev. B* **64**, 104419 (2001).
- <sup>21</sup>C. G. Zhong and Q. Jiang, *J. Phys.: Condens. Matter* **14**, 8605 (2002).
- <sup>22</sup>C. R. de la Cruz, F. Yen, B. Lorenz, Y. Q. Wang, Y. Y. Sun, M. M. Gospodinov, and C. W. Chu, *Phys. Rev. B* **71**, 060407(R) (2005).
- <sup>23</sup>H. D. Zhou, J. C. Denyszyn, and J. B. Goodenough, *Phys. Rev. B* **72**, 224401 (2005).
- <sup>24</sup>J.-S. Zhou, J. B. Goodenough, J. M. Gallardo-Amores, E. Moran, M. A. Alario-Franco, and R. Caudillo, *Phys. Rev. B* **74**, 014422 (2006).
- <sup>25</sup>Th. Lottermoser and M. Fiebig, *Phys. Rev. B* **70**, 220407(R) (2004).
- <sup>26</sup>P. A. Sharma, J. S. Ahn, N. Hur, S. Park, Sung Baek Kim, Seongsu Lee, J.-G. Park, S. Guha, and S.-W. Cheong, *Phys. Rev. Lett.* **93**, 177202 (2004).
- <sup>27</sup>A. V. Goltsev, R. V. Pisarev, Th. Lottermoser, and M. Fiebig, *Phys. Rev. Lett.* **90**, 177204 (2003).